

An X-ray microtomography study of particle morphology and the packing behaviour of metal powders during filling, compaction and ball indentation processes

Mozhdeh Mehrabi, Ali Hassanpour*, Andrew Bayly

School of Chemical and Process Engineering, University of Leeds, UK

ARTICLE INFO

Article history:

Received 19 November 2020

Received in revised form 22 February 2021

Accepted 24 February 2021

Available online 27 February 2021

Keywords:

Powder packing

X-ray microtomography

Ball indentation

Powder flow

Particle morphology

Additive manufacturing

ABSTRACT

The ball indentation method could be used to characterise powder packing and flow behaviours, particularly for the spreading stage of additive manufacturing (AM). However, there is no sufficient understanding of the powder packing state during the indentation process. In this paper, the X-ray microtomography has been used to characterise the particle morphology and visualize the packing behaviour of two grades of Ti6Al4V powders used in AM (gas atomized, GA, and hydride-dehydride, HDH), during the process of die filling (loose), consolidation (compacted) and ball indentation (indented). The packing fraction is found to slightly reduce under the indenter for GA powder (spherical shape) due to the dilation, while it does not change for HDH powder (irregular shape), suggesting it could be under a critically packed state. The packing fraction for both powders increases from central zone towards the wall due to the lower coefficient of friction for particle-wall than that of particle-particle.

© 2021 Elsevier B.V. All rights reserved.

1. Introduction

Additive manufacturing is a novel production route to create the component as a layer-based approach from the computer aided design (3D CAD) geometries by bonding layers of material using heat source or chemical binder [1]. It is an innovative production technology with flexibility and ability to generate a product quickly and less labour work for a unique and multi-functional shape component which is recently expanded in a wide range of industries such as aerospace, medicine and automotive [2]. However, there is still insufficient understanding of the effect of powder flow characteristics on the spreading behaviour within the AM process, which has a major impact on the quality of final products [3]. The smoothness and uniform packing fraction of the spread layer have great effects on bonding between particles-particles, layers and mechanical properties of final component [4]. Powder flowability is usually measured by universally well-known methods such as angle of repose [5], tapped density [6], Hall Flowmeter Funnel [7], FT4 [8] and shear cell [9]. However, producing a very thin layer of powders in AM process by using either blade or roller takes place under low consolidation stress thus it is essential to determine flowability and packing behaviour of powder as closely as possible to this condition. A comprehensive study has been carried out on different flowability techniques for powder both in dynamic and static state

conditions [9,10]. However, there is no specific method established to simulate the motion of bulk powder under the spreading process. [11].

A test method was introduced by Hassanpour and Ghadiri (2007) to characterise flow behaviour of powders, based on indentation of powder bed under low consolidation stresses [12]. In this method, a ball indented to the surface of consolidated powders, where the indenter maximum applied force and its projected area of imprint can be used to determine the powder hardness (H) using Eq. (1):

$$H = \frac{F_{max}}{A} \quad \text{Eq. (1)}$$

where F_{max} is the maximum applied load and A is projected area of the impression where can be obtained by Eq. (2):

$$A = \pi(d_b h_c - h_c^2) \quad \text{Eq. (2)}$$

where d_b is the diameter of the ball indenter and h_c is plastic deformation depth.

The indentation hardness gives the resistance of powder to plastic deformation under the specific force. Consequently, ball indentation has been successfully applied for assessing powder flowability for following materials: lactose, starch and Avicel [13], glass beads, Respitose SV003 and Fluid Catalytic Cracking (FCC) catalyst (commonly used in the petroleum industry) [14] and calcium carbonate (Durcal 15) and limestone [15]. They showed that the ball indentation results correlate

* Corresponding author.

E-mail address: a.hassanpour@leeds.ac.uk (A. Hassanpour).

very well with common flowability measurement techniques by applying a “constraint factor” (C), the ratio of indentation hardness (H) to the yield stress (Y), ($H/Y=C$), which depends on single particle properties such as size, shape, roughness and coefficient of friction. However, the hardness measurements could also be affected by the distribution of packing fraction of loose and consolidated powder bed at different compaction stresses, wall effects and segregation of particles during filling and consolidation, which are yet to be studied in detail.

X-ray microtomography (XMT) is a non-destructive, relatively fast and accurate method which can reveal detailed information of the internal 3D structure of objects. Recently, it has been utilised for dimensional measurement and porosity analysis of internal structure of complicated components in AM process [16]. In recent years there have been various research works analysing the metal powder feedstock using high resolution micro CT from single particle characterisation [17,18] to study the effect of the grade of metal powder on porosity and quality of final components [19].

It also could be said that this is main method for high-quality and detailed analysis of single particle physical properties such as sphericity, surface area, volume and aspect ratio, which all have significant effect on the quality of powder bed. Shape characterisation of particles has been historically studied by electron microscopy and more recently XMT [20,21].

There have been a number of attempts in establishing relationship between particle size and shape and flow characteristics [22]. Bumiller et al. [23] used shear cell for assessing the flow properties of glass sphere, calcium carbonate crystal and plate shape talc powder and suggested that particle shape might have significant effects on powder flow properties. Podczek and Mia [24] investigated shear properties of 8 different powders with different size and shape and they concluded the particle size and shape have great influence on powder flow factor and internal angle of friction. Yu et al. [25] conducted numerical simulations of the bulk powder flow for powders with various particle size and shape distributions and stated that both particle size and shape play important roles in determining the powder flow behaviour. All these researches emphasise on the effect of both particle size and shape on shear parameters, flowability (spreadability), however systematic and in-depth studies for irregularly shaped particles utilising three-dimensional shape analysis (e.g. by XMT) for this purpose are limited.

Chawanji et al. [26] implemented XMT for the study of packing efficiency of two different milk powders under specific load and attributed their different behaviour to the particle properties. They found that the packing efficiency is higher for powder containing surface fat which acts like lubricant and reduce particle-particle friction and leading to closer packing.

XMT has been used extensively to study particle behaviour during die compaction. Particularly McDonald et al. [27], worked intensively on the effect of different punch shapes (flat, angled and rounded) on the rearrangement and movement of 0.5 mm glass spheres during compaction by using XMT. The study focused on the shape of different punches on localised density around the indenter and but the effect of size and shape of particles on the packing density was not the subject of the study. They followed the work by studying the particle movement during compaction of blended aluminium and tin powders with size distribution of 38–45 and 125–140 μm , respectively. They reconstructed the tomographic images with voxel size of 27 μm and but could only track the local pixels of tin particles at different stage of compaction, presumably due to the small size of aluminium particles. A dimensional displacement maps around the compaction punch and the localised density fraction were reported [28]. The in-situ shear deformation of aluminium powder during compaction and the formation of shear crack have also been demonstrated [29], however, individual particles in the whole powder bed were not visualized and the quantitative analysis of radial and axial packing fraction for the entire bed and the wall effects for specific applications such as ball indentation were not reported.

Numerical modelling of powder packing density and die compaction during ball indentation has also been studied which provided great insight of the process [30,31]. Although the powder shear zone around the ball indenter has been numerically studied to find the shear stress and the effect of constraint factor in confined powder bed, no experimental work has been reported on the three-dimensional visualization of powder packing behaviour during the ball indentation process.

Therefore, the aim of this research is to carry out, for the first time, a three-dimensional analysis of the ball indentation process using XMT in order to develop better understanding of the powder packing behaviour during the process. The powder flow behaviour during the indentation process is dependent on conditioning and packing configuration of the powder bed which can be studied using XMT. In this work XMT is used to analyse the shape and size of two grades of powders of the same material but with different physical properties, and to investigate their packing density variation in different regions of the powder bed as a result of consolidation and indentation processes.

2. Experimental procedure

2.1. Materials

In this work two grades of Ti6Al4V powders produced from different manufacturing processes, (i) Hydride-dehydride (HDH) irregular shape particles (Fig. 1a) and (ii) Gas Atomised (GA) spherical particles (Fig. 1b), have been investigated to compare their packing behaviour.

The particle size distribution of both powders was measured using laser diffraction technique (Mastersizer 2000) and is reported in Fig. 2. It can be seen that based on laser diffraction technique, the particle size of HDH ($D_{50} = 92 \mu\text{m}$) is measured larger than GA ($D_{50} = 64 \mu\text{m}$).

The chemical compositions (determined using Energy Dispersive X-ray, EDX) and the true density (obtained using Thermo Scientific™ Pycnomatic ATC) of both powders are presented in Table 1 and Table 2, respectively.

2.2. Experimental setup

To investigate the packing density for loose and compacted powder and visualize the powder bed behaviour during ball indentation, the X-ray micro tomography (MicroXCT, Xradia Versa 410) at the University of Leeds was used.

The experimental rig included a die (10 mm diameter cylindrical die with 15 mm depth), a piston (10 mm diameter), a ball indenter (4 mm diameter) made of glass and a set of weights to allow a range of consolidation forces to be tested. The die and the piston were made of poly methyl methacrylate in order to ensure minimal attenuation of X-ray during capturing of projection slides for the rig (Fig. 3).

Initially the die was fully filled with powder GA (3.10 g) and HDH (2.50 g) with the “sieved method”, where the sample was passed through a sieve with the mesh size 5 times the D_{50} of the samples ($5 \times D_{50}$) directly above a funnel on top of the die to get the uniform loose randomly packed powder bed [15]. Then it was mounted on the rotating sample stage with a high level of care (Fig. 4a). Then x-ray with photon power of 140 kV and current setting of 70 μA were used to acquire series of projection images as sample was rotating. These projection images were used to reconstruct the volumetric data (Fig. 4b) (Fig. The magnification or final voxel size in reconstruction of volume is dependent on the distance between the x-ray source and sample holder (Table 3).

The first scan was performed on the initial state of loose particles, where their rearrangements could be affected by their properties such as shape, weight and particle-particle and particle-wall friction.

Then second scan was performed after mounting the piston with 120 g weight at the top applying a pressure equal to 14.9 kPa. In this study, a relatively high consolidation stress was used because during

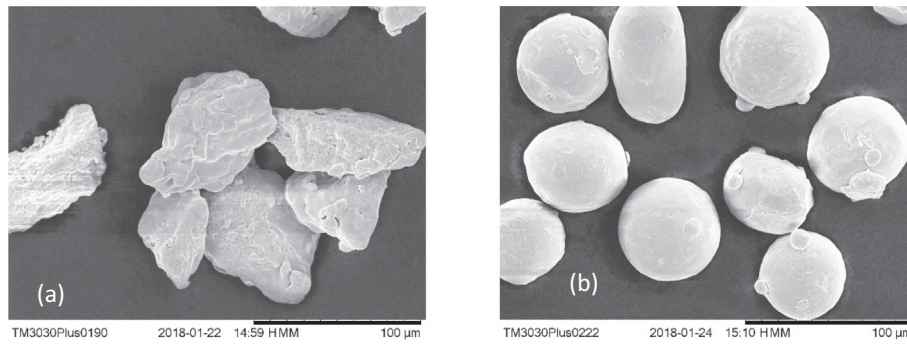


Fig. 1. SEM images of (a) Hydride-dehydride (HDH) and (b) Gas atomization (GA) of Ti6Al4V samples.

ball indentation the weight of in-situ ball indentation set up (sliding rod attached to the ball) is relatively large and that would have led to an excessive penetration, if a low consolidation stress was used. Also, to minimize any undesirable particle disturbance due to the movement of sample holder, the piston was placed on the sample while it was inside the x-ray device.

For the last scan, the load was removed, and the ball indenter was placed carefully on top of the powder bed, then it was lowered under its own weight (1.01 g equal to 9.9mN). For each of the three different stages of “loose, compaction and indentation”, the x-ray micro tomography settings were kept constant to ensure similar resolution and region of interest.

All the measurements were conducted at a constant temperature of 25 °C inside the chamber with relative humidity of about 40%.

2.3. Data analysis

The 3D reconstructed volume of the whole sample was characterized by the Avizo® software. Initially, images were subjected to sharpening and edge detecting filter to remove a substantial level of noise while preserving the edge of each particle (Fig. 5). Then they were segmented manually into binary format based on the distribution of greyscale of each pixel value to separate the individual particles from the void (Fig. 5b). Different phases of particles and voids filled by the air in radiograph images of XMT are indicated by different greyscale intensities, due to the variation of x-ray absorption related to physical density and atomic mass of the object, which can be seen in voxel intensity histogram [35].

Table 1

The elemental composition of the samples GA and HDH by EDX.

Element	GA Wt%	HDH Wt%
Ti	89.6	89.35
Al	6.23	6.57
V	4.17	4.07
Total	100	100

Table 2

True density of both samples.

Powder	True Density (g/ml)
GA	4.44
HDH	4.47

User dependency is the basic limitation of thresholding technique. To make sure that the range of binary segmentation is correct, the quantitative results should be comparable with known parameters (e.g. density) obtained by different methods. To ensure accuracy of determination of individual particles with their internal details and their edges, the whole sample packing fraction (PF) given by the software (Eq. 2) after binarization was compared with the calculated packing fraction of powders from its volume (from height of sample in the die), weight and true density [33] (Eq.3). Then the range was chosen by considering the error ($\pm 0.001 \text{ g/cm}^3$).

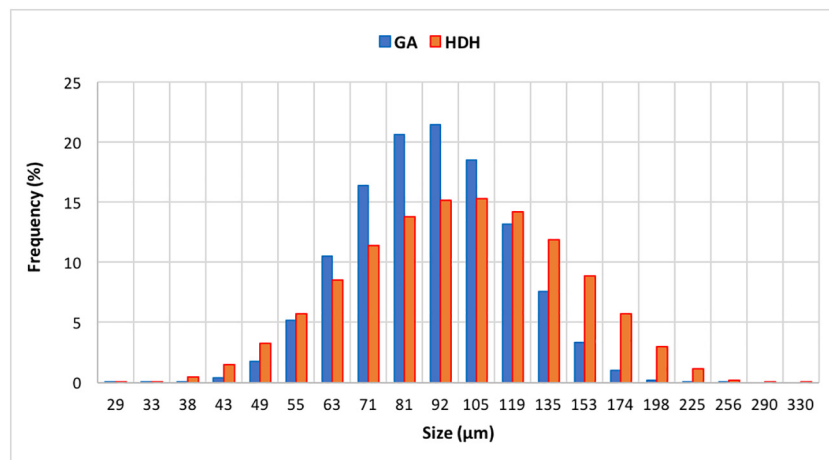


Fig. 2. Size distribution of GA and HDH powders measured by laser diffraction.

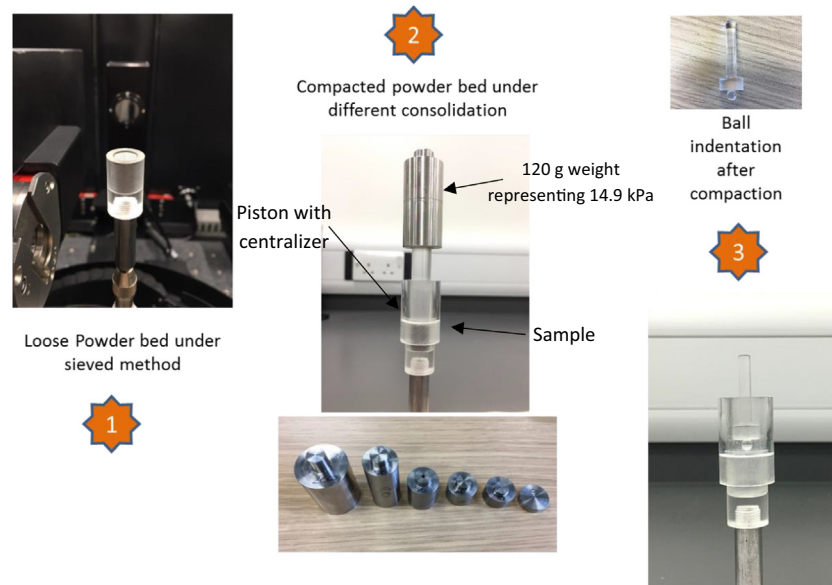


Fig. 3. Sample preparation for three stages of indentations during X-ray micro tomography.

$$\text{PF from Avizo software} = \frac{\text{Volume occupied by particles after thresholding}}{\text{Volume of whole sample}} \quad \text{Eq. (3)}$$

$$\text{PF from calculation} = \frac{\text{Density measured by weight and volume of sample}}{\text{Material density (single particle true density)}} \quad \text{Eq. (4)}$$

To separate particles in order to calculate their equivalent diameter, volume, sphericity and other shape parameters, the “watershed segmentation” has been used. This concept has been used in several applications such as medical, soil and powders [36–38]. Fig. (6) illustrate the concept of “watershed segmentation”. The binary image indicates two particles in contact with known radius (Fig. 6a). In Fig. 6b two local “minima” can be identified and therefore the “watershed line” can be placed between the particles in contact (Fig. 6c) from which the “catchment basins” can be used to separate particles.

In this research, to improve the quality of segmentation the “marker-controlled watershed” method was used, which has been applied for several applications [39,40]. The “marker control watershed” is for modification of vicinity of local minima to improve the precision of defining catchment basin and segmentation.

The first step of this method for separation is to construct the binary image of particles by choosing the binarization range which indicates particles in contact (Fig. 7b). The second step is “distance transformation” to define the minima for individual particles, i.e. the bright voxel

representing the particle grain, from which the particle boundaries could be identified (7c). Then the distance transformed image is processed by the “H-maxima” (defining a filter limit for minima) to modify number of local minima to minimize/eliminate over segmentation (7d). The next step involves watershed segmentation, where the whole image is considered as topographic surfaces according to the method described earlier (Fig. 6) to identify the “catchment basins” (Fig. 7e) from which particles can be separated and labelled for further analysis (Fig. 7f). This works reasonably well for round particles [39] while for highly irregular shapes there could be more than one minima for each object which makes the separation of wide size distribution particles very challenging [38].

Wang et al. [39] established that the best results for “marker-based watershed” segmentation is obtained for particles with the size to voxel size ratio of bigger than 30 which is the case for particles used in this study. However, there is a potential error in the above mentioned method, which increases for irregular shape particles, i.e. the HDH sample in this work, making the method unsuitable for the separation which detects several local minima for each individual particle, leading to over-segmented images [41,42].

In this work, in another sets of measurements the particles were placed in cotton filled sample holder to make sure they are separated and not touching each other. Then the results for both methods were compared. For GA powders there has been an excellent agreement between the d_{50} of particle obtained by the two methods, indicating the “marker-controlled watershed” is feasible to separate the particles

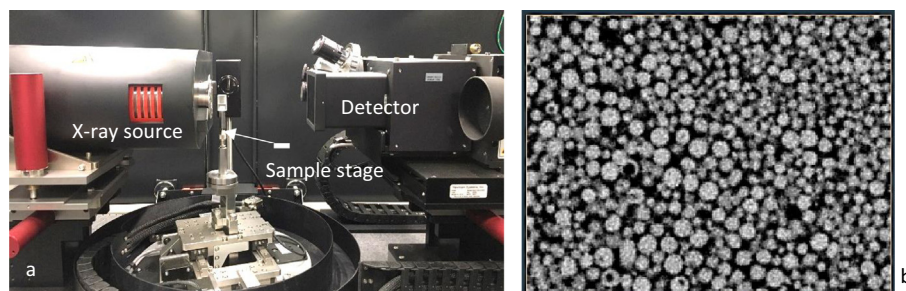


Fig. 4. XMT (a) set up, (b) reconstructed image of sample GA.

Table 3
Acquisition conditions and parameters of XMT.

X-ray Device	Voltage (kV)	Current (μA)	Filter	Exposure time (s)	Number of projections	Voxel size (μm)
Zeiss Xradia Versa	140	70	HE2	12	1600	7.4

(Fig. 8). However, for HDH, the results of the two methods were not comparable, making the “marker-controlled watershed” method unsuitable for individual separated particle analysis.

3. Results and discussions

3.1. Particle shape analysis

Firstly, individual particles (more than 20,000 particles) for both samples were analysed for their shape factors such as “sphericity” (Ψ), “aspect ratio” (AR) and “equivalent diameters” (based on both volume and surface area). For GA powder the watershed segmentation which was described in previous section was used to analysis particles from different part of the bed while for HDH powder due to limitation of segmentation method, the powder spread through the cotton sample holder has been analysed. Examples of individual particles can be seen in Fig. 9 for both samples. At glance, it can be observed that GA particle has more roundness and its surface is smoother as compared to the HDH particle which shows an irregular elongated shape with a high degree of surface roughness. Further detailed quantitative shape analyses of the powders are given in the following section.

Based on the XMT image, a triangular mesh from the Marching Cube method can be reconstructed to provide the volume and the surface area of the particle [43]. Once the triangular mesh surface of the particle is reconstructed, the equivalent diameter is based on physical properties of particles such as their volume or surface area can be determined.

For non-porous particles, the equivalent spherical diameter is the measurement which is commonly used [44]. This can be reported as the “volume equivalent sphere diameter” (D_v), the diameter of sphere with same volume as the particle volume, or the “area equivalent sphere diameter” (D_a), the diameter of a sphere with the same surface of particle. The results for GA and HDH powders based on both diameters are presented in Fig. 10. It can be seen that HDH powder has larger particle size than GA which is also shown by the laser diffraction technique (Fig. 2). However, overall laser diffraction measurements result in bigger equivalent sizes than XMT measurements (D_v). For GA powder the difference between the laser diffraction and XMT measured sizes (D_v) is smaller than that of HDH, presumably due to a more regular shape for GA particles. that For GA

As would be expected for non-spherical particles there is a difference between the distributions based on the two diameter definitions. As well as overall particle shape, there is a contribution from surface pores and satellite particles in the case of GA powders and the surface roughness of HDH particles.

Sphericity (Eq. 5) was measured by the ratio of surface area of a sphere with same volume as the given particle to the surface area of the particle using the correlation shown below:

$$\psi = \frac{\pi^{1/3}(6V_p)^{2/3}}{A_p} \quad \text{Eq. (5)}$$

Where V_p is volume of given particle and A_p is its area.

As can be seen from Fig. 11, majority of GA powders have nearly spherical shape unlike the HDH powders. Some GA particles have satellites (e.g. in Fig. 12a) with the sphericity in range of 0.8 to 0.9. In addition, there are occasional concave shape (e.g. Fig. 12b) as well as nearly spherical but hollow GA particles (e.g. Fig. 12c–12d) with the sphericity ranging from 0.6 to 0.8.

For instance, the particle in Fig. 12c is nearly spherical but because it is porous, its equivalent volume diameter used in the numerator of Eq. 5 would be underestimated because the particle volume (V_p) is reported

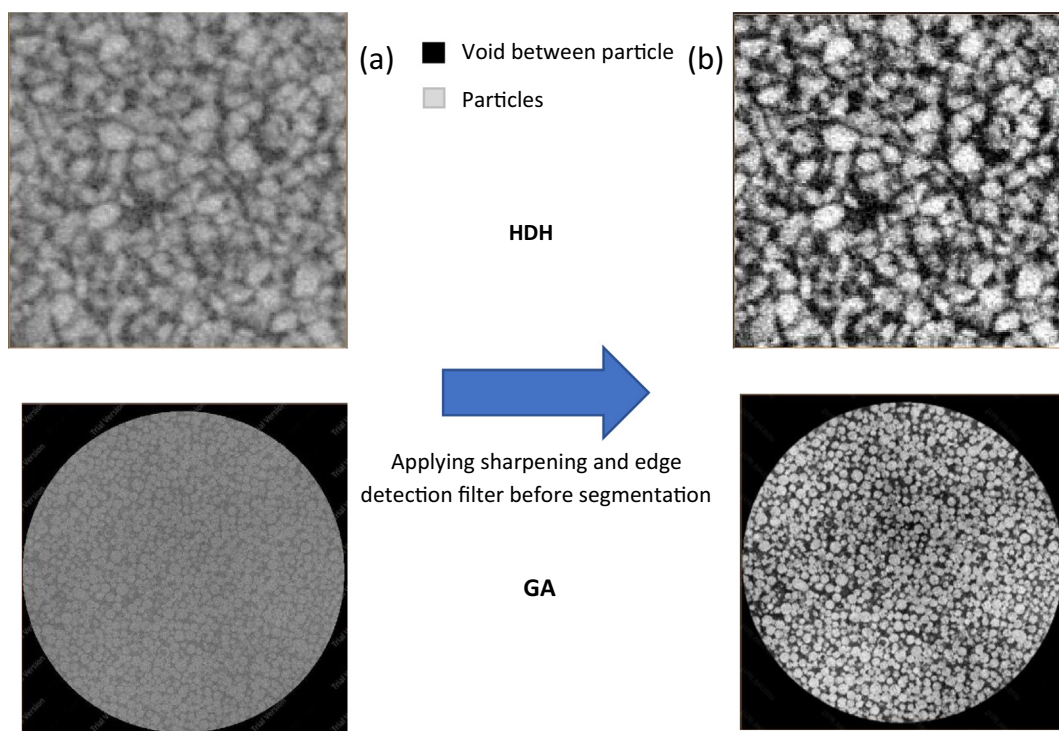


Fig. 5. (a) Before and (b) after sharpening filter on sample HDH.

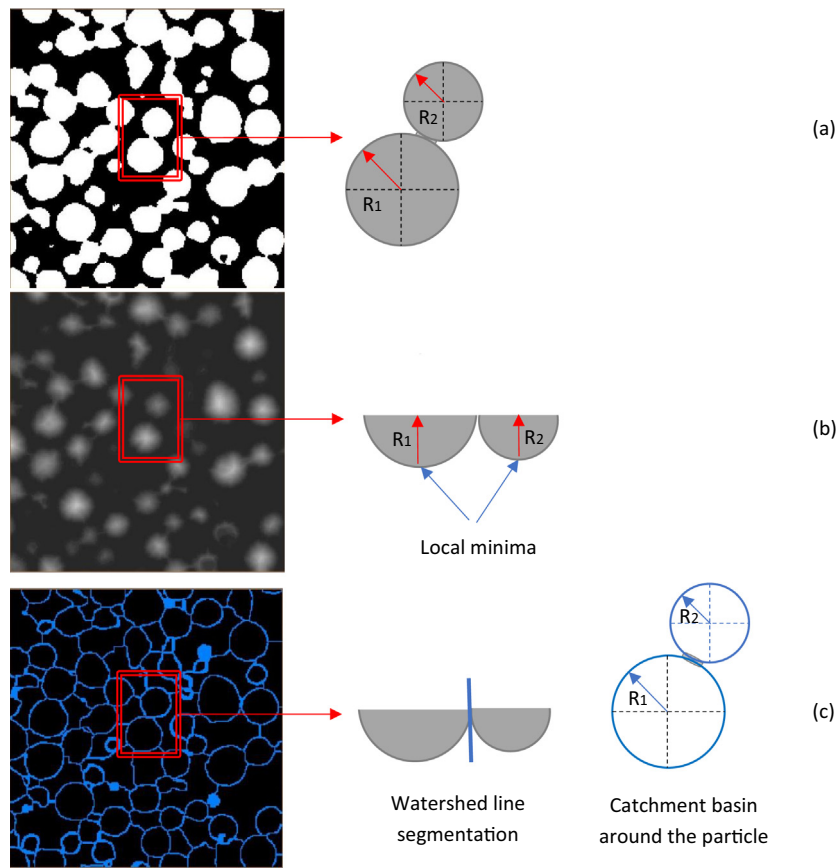


Fig. 6. Illustration of watershed segmentation.

by the image analysis software as the total volume of voxels (excluding the pores). This will result in a smaller sphericity (0.85) while for similar particle (similar dimension) without the pore, its envelope sphericity is found to be 0.98 (Fig. 13).

It is worth mentioning Liu et al. [45] characterized different shape factors for Ti6Al4V powders using the SEM images and reported that

for GA particles the average roundness and elongation are 81 and 84%, respectively, while 48% of particle had satellites [45]. The analysis in this work would provide complementary information on the 3-dimensional structure of the powder.

The aspect ratio of a particle is the ratio of its smallest Feret dimension (d_{\min}) to the largest Feret orthogonal (d_{\max}) as given below:

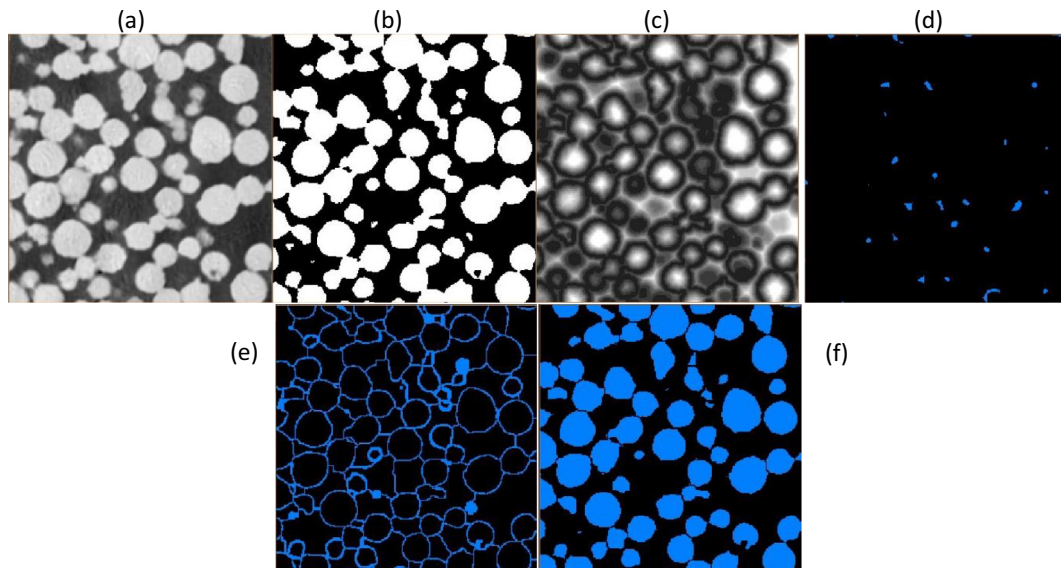


Fig. 7. Steps of digital separation of particles. (a) Original greyscale image of powder GA, (b) initial binary images of attached particles, (c) distance transformation, (d) H-maxima transformation, (e) image after watershed segmentation line, (f) separated particles.

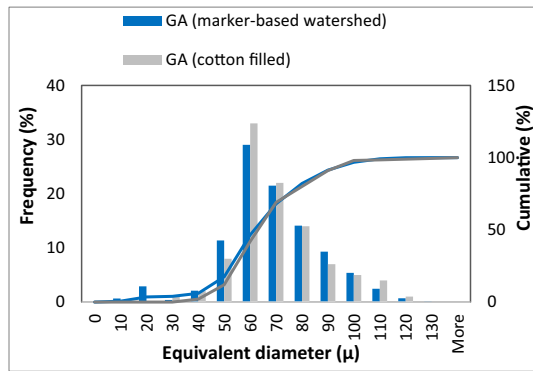


Fig. 8. Comparison of the cotton filled and marker-based watershed segmentation methods to characterise the particle size distribution.

$$A_R = \frac{d_{min}}{d_{max}} \quad \text{Eq. (6)}$$

It is qualitatively obvious by the SEM images (Fig. 1) that HDH particles are more elongated as compare to GA particles, which is also confirmed quantitatively, from their aspect ratio results in Fig. 14.

Except some irregular GA particles which have aspect ratios in the range of 0.4 to 0.7 (e.g. in Fig. 15a–15b), the aspect ratio for the majority of GA powders (68%) is within the range of 0.8 to 0.9 with few occasional satellites (Fig. 15c–15d).

For comparison, few hollow (with blind/ enclosed pore) and concave particles are manually selected and presented in Fig. 16. For hollow particles despite their “envelope” spherical shape, the calculated sphericity (true sphericity) from Eq. 5 ranges of from 0.70 to 0.85 depending on their pore sizes. Bigger porosity results in smaller “true” sphericity. However, such particles have high aspect ratio which is not necessarily indicative of their true shape. Hence, care must be taken when comparing particle shapes based on the above parameters.

For concave particles the aspect ratio could not be a good shape indicator. There are particles with high aspect ratio that have a small sphericity due to existence of their concave hole.

Some particles have smaller equivalent diameters (D_v) than their three-dimension axes (length (L), width (W), thickness (T)), which can be found for both hollow and concave shape particles.

Size and shape of internal porosity could result in defects in AM built parts which are known as the most critical flaws in regard to the mechanical strength and component toughness [46].

3.2. Volume fraction

To calculate the “packing fraction” for loose, compacted and indented samples, the pixels area occupied by particles were obtained

for each projection slide and used for the calculation of the total packing fraction. Fig. 17 shows the x-ray image of loose state of the powders filled by the sieving method [15] followed by the compacted and indented powder bed for both samples. It can be observed that the indenter penetrated more into the compacted HDH powders which could indicated to a less consolidated state as compared to that of GA powders.

The regions of interest for the quantitative comparison of packing density in both radial (inner, outer and wall) and central zones through the bed have been chosen for all three stages (loose, compacted and indented) (Fig. 18). The radial zones have the same width and length (1110 and 850 μm, respectively) going from top to bottom of the bed (Fig. 17). Each radial zone is the average of 4 separated sections as shown in Fig. 18. The central zone is exactly the under the ball but it is chosen larger than other sections to cover the plastic deformation zone underneath the ball. All average packing fraction values for each zone are presented in Fig. 19.

The overall average packing fraction (percentage) as well as those of individual radial zones for loose, compacted and indented states are compared for both samples in Fig. 19. It can be seen that HDH has lower overall packing fraction than GA for all three stages. However, for both samples the packing fraction of the loose stage increases from the central zone towards the wall. This variation reduces after the compaction stage for both samples, where a reduction of the packing density is observed near the wall after the compaction (more significant reduction for HDH than GA) as opposed to other zones where an increase in packing fraction is seen. After indentation, the packing density reduces in all zones for GA powders, while this reduction is only observed around the wall for the HDH powders.

Overall the GA powders have a higher packing fraction than HDH powders due to their size, shape and surface roughness. Specially at loose stage which powders do not undergo of compaction, GA particles with higher sphericity and aspect ratio tend to get higher packing fractions [47,48]. While the HDH particles with irregular shape would tend to interlock leading to smaller packing percentage. Hence, they could tend to have more block movement when they are being indented which could result in smaller or no change in the packing fraction. This could resemble a behaviour of powders with a critical state of consolidation.

The frictional interaction between the particles and particles and the wall could affect the packing pattern of the powders. If the particle-wall friction is smaller than that of particle-particle, during loose-packing, particles are settled easier near the walls according to their nature (size and shape), hence the packing fraction becomes higher close to the wall, while in the middle zone the interlock of particles results in less packed density fraction. This observation has been reported by previous researchers using a destructive experimental approach (embedding the compact in resin and slicing) [53] as well as computer simulation [54]. In order to test this hypothesis for GA and HDH

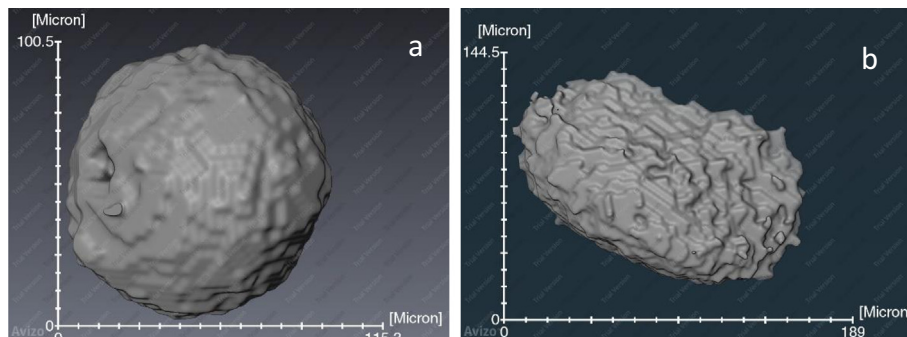


Fig. 9. Close up images of reconstructed particles (a) GA and (b) HDH.

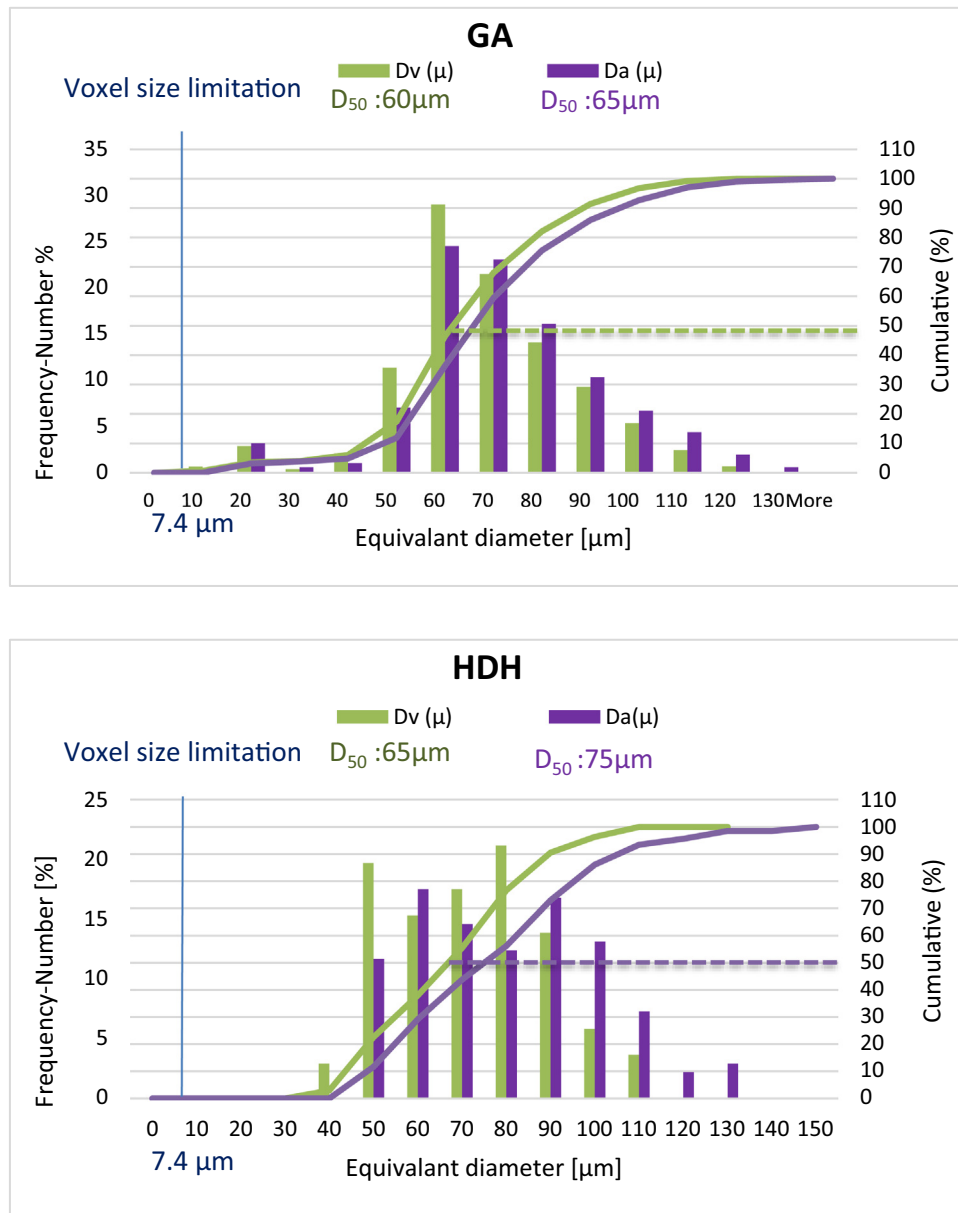


Fig. 10. Comparison of equivalent diameter extracted from Volume and surface area of 20,000 individual particles.

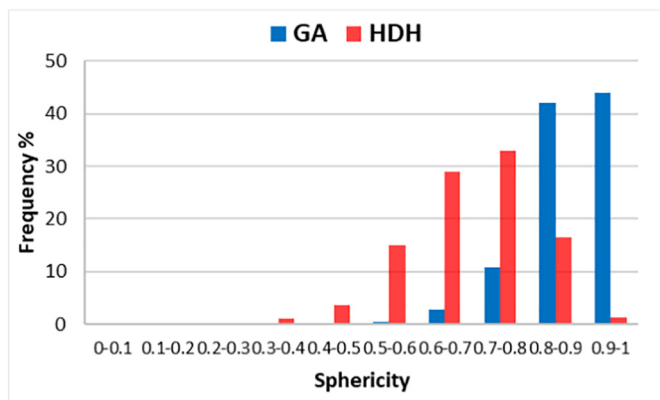


Fig. 11. Sphericity of GA and HDH samples.

powders, the “coefficient of sliding friction” (CoF) between particle-particle and particle wall was experimentally measured for both samples [49]. For particle-particle CoF measurement, a thin layer of super glue was applied to two separate surfaces (Perspex, same material as the die and piston) (Fig. 20), then the powders were gently deposited on the surfaces. The surfaces were placed on top of each other and tilted until the sliding angle was detected (Fig. 21).

For the measurement of particles and wall CoF, the same process is applied but a plane lower surface is used instead of that of adhered particles. The results of CoF for both particle-particle and particle-wall are calculated by Eqs. 7 and 8 and presented in Table 4. Each test was repeated until the average and Standard Deviation did not change significantly. This was achieved after 10 repeats.

$$\alpha = \sin^{-1} \frac{A}{B} \tag{Eq.(7)}$$

$$COF = \tan \alpha \tag{Eq.(8)}$$

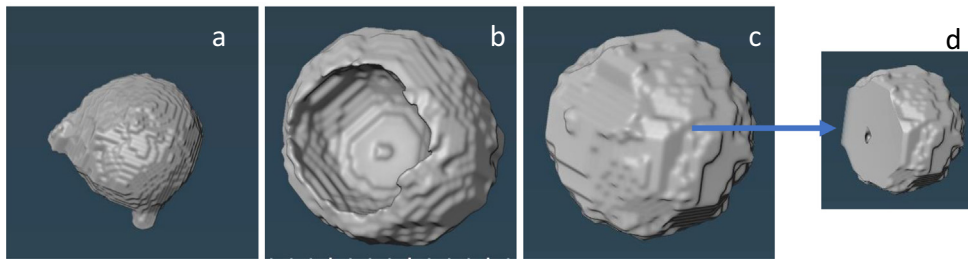
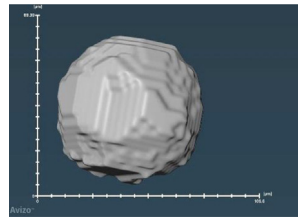


Fig. 12. Different shapes of GA particles particle with satellite (a), concave particle (b), porous particle (c) and cross section of particle c (d).



Length (μm)	Thickness (μm)	Width (μm)	sphericity
83.34	75.12	72.63	0.98

Fig. 13. Particle GA with dimensions and its sphericity.

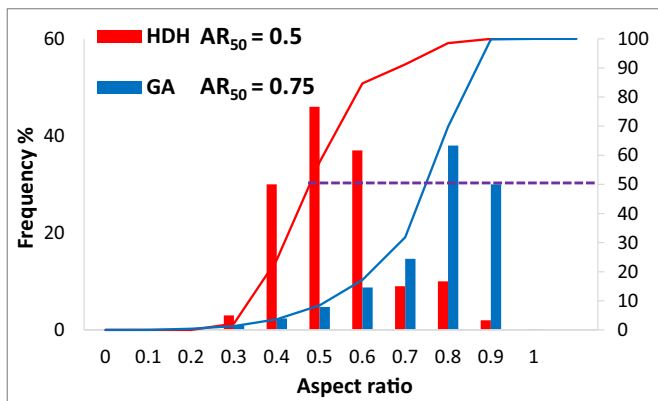


Fig. 14. Aspect ratio of GA and HDH samples.

It can be observed that indeed the particle-wall CoF is lower than that of particle-particle for both samples, hence leading to a higher packing towards the wall according to the aforementioned theory. These results are correlating well with internal angle of friction of both samples extracted by shear cell results.

The axial variation of the packing density has also been analysed for both samples. In particular, the axial variation for central zone (around indentation point) and that of wall zone are shown in Fig. 22 for both samples. For GA powders as presented in Fig. 22a, it can be noticed

that the trends of axial variation of packing densities are very similar, all the way from top to the bottom, for all three stages. At loose stage powders rearrange due to their weight and physical properties for which a trend is formed. When powders undergo compaction, with constant pressure on the bed, the packing density increases, but keeps a similar axial trend as that of the loose stage. Once the compaction pressure is removed and indentation stage takes place, it can be observed that the packing fraction is reduced but here again with the same trend as those of compaction and loose stages, except near the top, just below the indenter, where there is further reduction in packing fraction due to the dilation of powder to accommodate shear under the indenter. It should be noted, after removal of compaction pressure, before the indentation stage take place, there could be a degree of elastic recovery for the powder bed [50,51] which could also contribute to the reduction in packing density.

Fig. 22b shows the axial variation of packing density for GA at the three stages in the zone close to the wall. It can be observed that GA powders have high packing density near the wall at loose stage due to their small powder-wall friction (as described earlier) but with little reduction after the compaction stage followed by further reduction after the indentation. Here, the axial trend in packing fraction is not entirely similar for the three stages, unlike the central zone. It is interesting to note that there is a significant drop of packing fraction close to the bottom-corner of the die. This phenomenon can be observed for HDH powder as well (Fig. 22d).

Fig. 22c shows the axial packing fraction for HDH powders in the central section at loose, compacted and indented stages. Similar trends

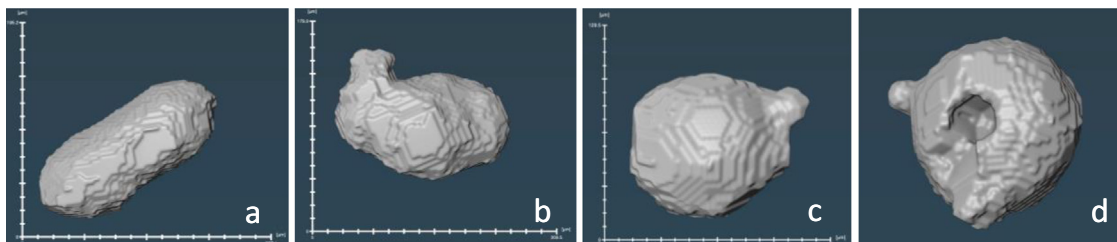


Fig. 15. GA particles with 0.4 to 0.8 range of aspect ratio (AR); (a) AR = 0.43 (b) AR = 0.57 (c) AR = 0.70 (d) AR = 0.83.

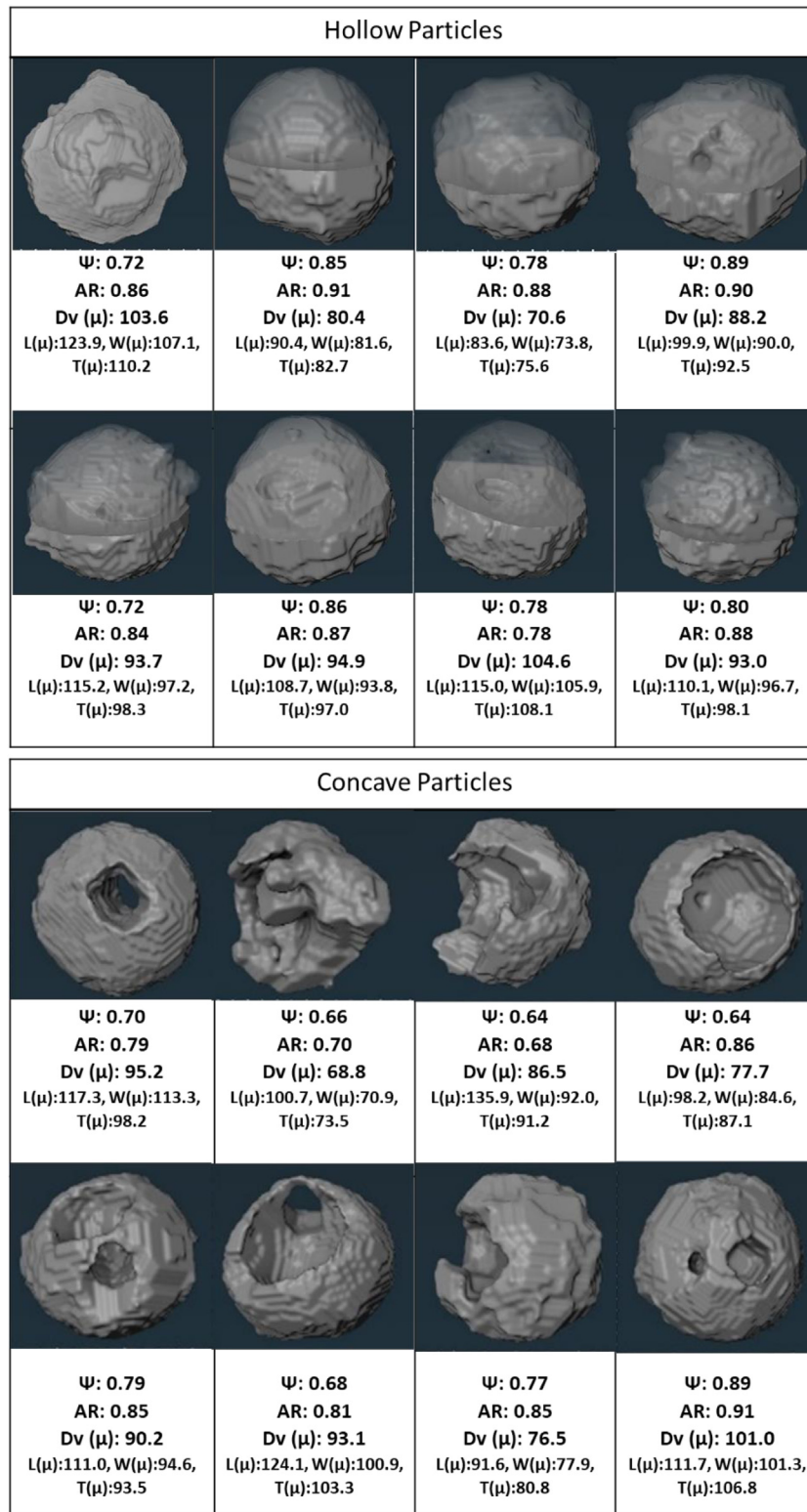


Fig. 16. Comparison of hollow and concave particles for their sphericity, aspect ratio, porosity and diameters.

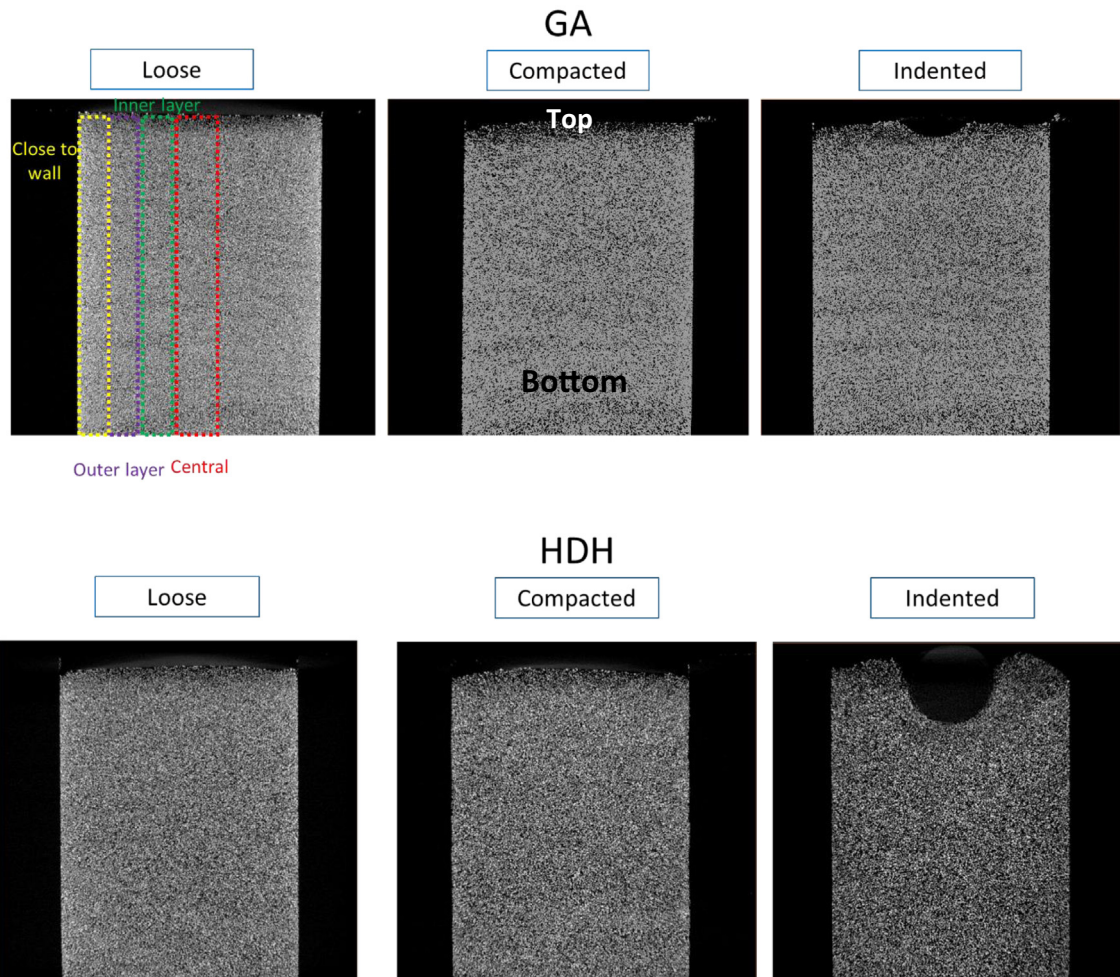


Fig. 17. 2D Axial greyscale slide through the 3D volume for each test (Loose-Compacted-Indented) of GA and HDH powders.

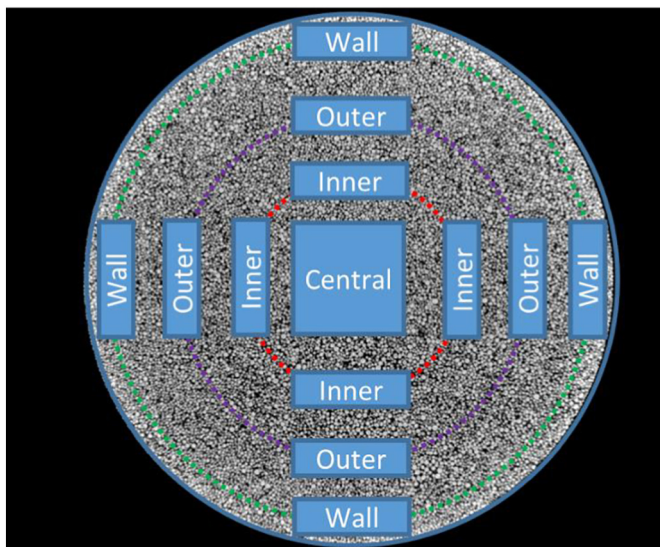


Fig. 18. 2D Cross section slide of HDH powder with region of interest.

for axial packing fraction are observed for loose and compacted stages, while for the indentation stage, where overall HDH exhibits no significant change in packing fraction, there is a degree of rearrangement of

particles which leads to different axial trend compared to the loose and compacted stages. As opposed to GA powders, HDH powders did not show the dilation of powder (reduction in packing fraction) under the indenter suggesting the powders could be under a critically packed state presumably due their irregular shape (Fig. 22c). It should also be noted that the indenter has penetrated more into HDH (2.6 mm) as compared to GA powders (1.4 mm) and this might also be affecting the observed packing behaviour for the HDH powders.

It should be noted that the critical packed state determines whether powder tends to retain the same void fraction during shear deformations. In dense (over consolidated) powders the bed reaches the critical state as a result of dilation, while in loose packing it tends to reach the critical state after a volumetric contraction.

Fig. 22d lays out the packing density of HDH powders in the zone close to the wall. The packing fraction reaches to the highest level at the loose stage and shows more significant reduction after the compaction. There is a sudden drop in packing density at all stages near the bottom corner, with somewhat a higher extend as compared to GA powders.

The above analyses show that at loose stage, GA powder in the central zone has the same packing fraction as the HDH powder close to the wall zone (ca 57%), indicating that for loose or very low compaction stages, the radial position of indent would significantly influence the powder bed hardness measurement. This is due to the difference between the particle-particle and particle-wall frictions for the two powders investigated in this study. Furthermore, the trend of packing

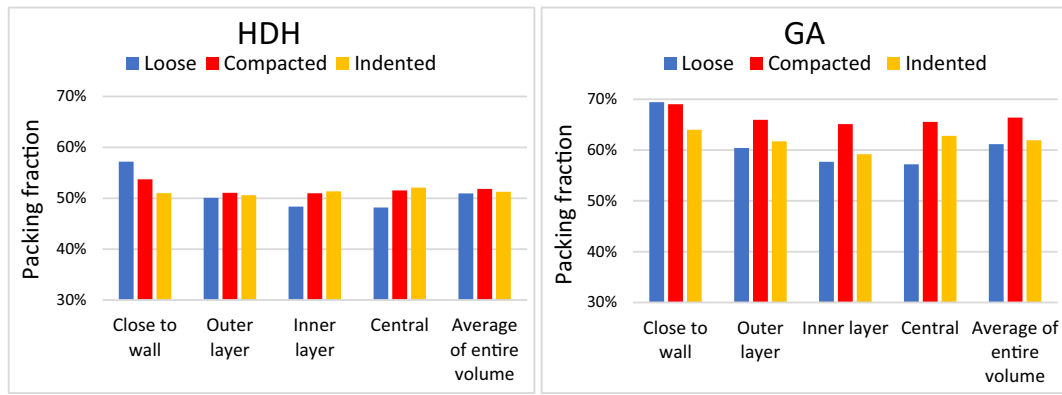


Fig. 19. HDH and GA Powders packing fraction for loose, compacted and indented samples.

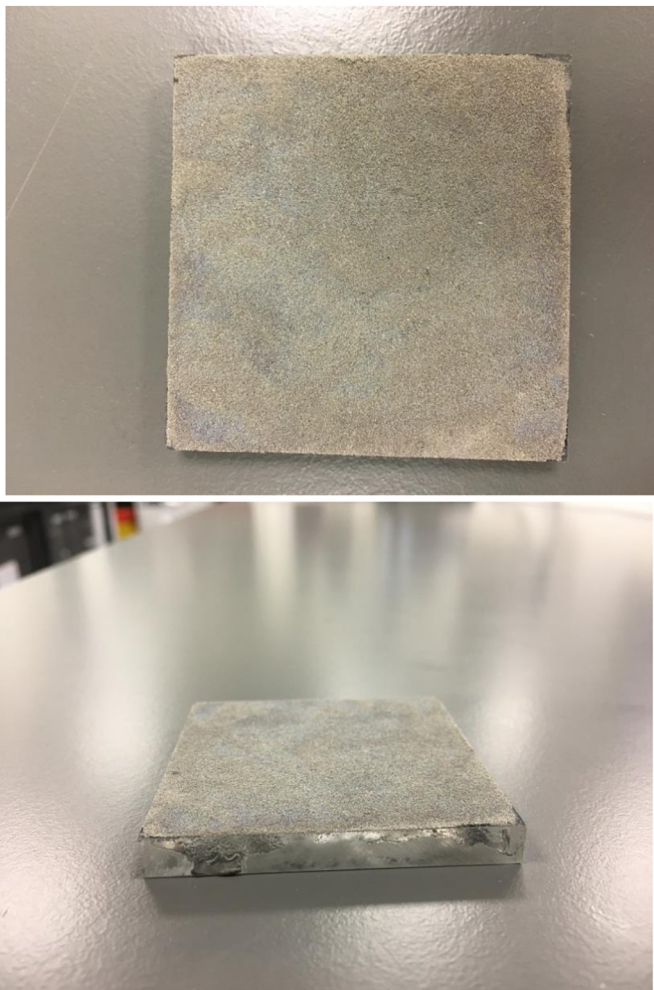


Fig. 20. Image of prepared sample adhered to a surface for measuring CoF.

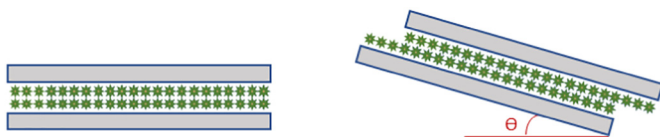


Fig. 21. Schematic diagram for measuring CoF between particle-particle.

Table 4
Sliding friction of GA and HDH powders.

	Coefficient of sliding friction (μ)	
	Powder-Powder	Powder-Wall
HDH	0.87 ± 0.038	0.25 ± 0.009
GA	0.47 ± 0.062	0.19 ± 0.019

fraction under the indentation zone could be an indication of critical state of the powder compaction for the HDH powders as opposed to GA. This could have significant influence on the value of constraint factor for the calculation of powder yield stress [31–52] from hardness measurement which is mainly due to the particle re-arrangements under the indentation zone as affected by the particle shapes and coefficient of frictions.

The study in this work demonstrates the different packing behaviours of the two grades of Ti6Al4V which is caused by their different morphologies. This difference would have an influence on the spread layer quality during the AM process which could have impact on the quality of final product. Powder packing density is a crucial feedstock parameter which determines how efficient particles arrange themselves with maximum particle-to-particle contact and minimum voids within the granular network. It is very critical that each powder layer have uniform thickness and density as a high porosity or uniform layer could lead to weaker bond between layers and poor mechanical properties of final products. Overall HDH powder has less packing fraction after consolidation compared to GA, which could result in smaller bed hardness. However, irregular particles (HDH) would have less freedom due to the interlocking phenomenon which reduces their individual mobility. This could have a significant influence on the quality of spread later during the process of spreading for AM.

4. Conclusions

The purpose of this study was to characterise physical properties of two different grades of Ti6Al4V metal powders, namely GA and HDH, and carry out an internal visualization of the filling, compaction and ball indentation processes of powders by the x-ray microtomography, in order to develop better understanding of the powder packing behaviour and effect of consolidation pressure and ball indentation on powder bed. The following conclusions could be drawn from this work:

- The shape analysis has revealed that the GA powders have nearly spherical shape while the HDH powders have rather irregular shape with surface asperities.

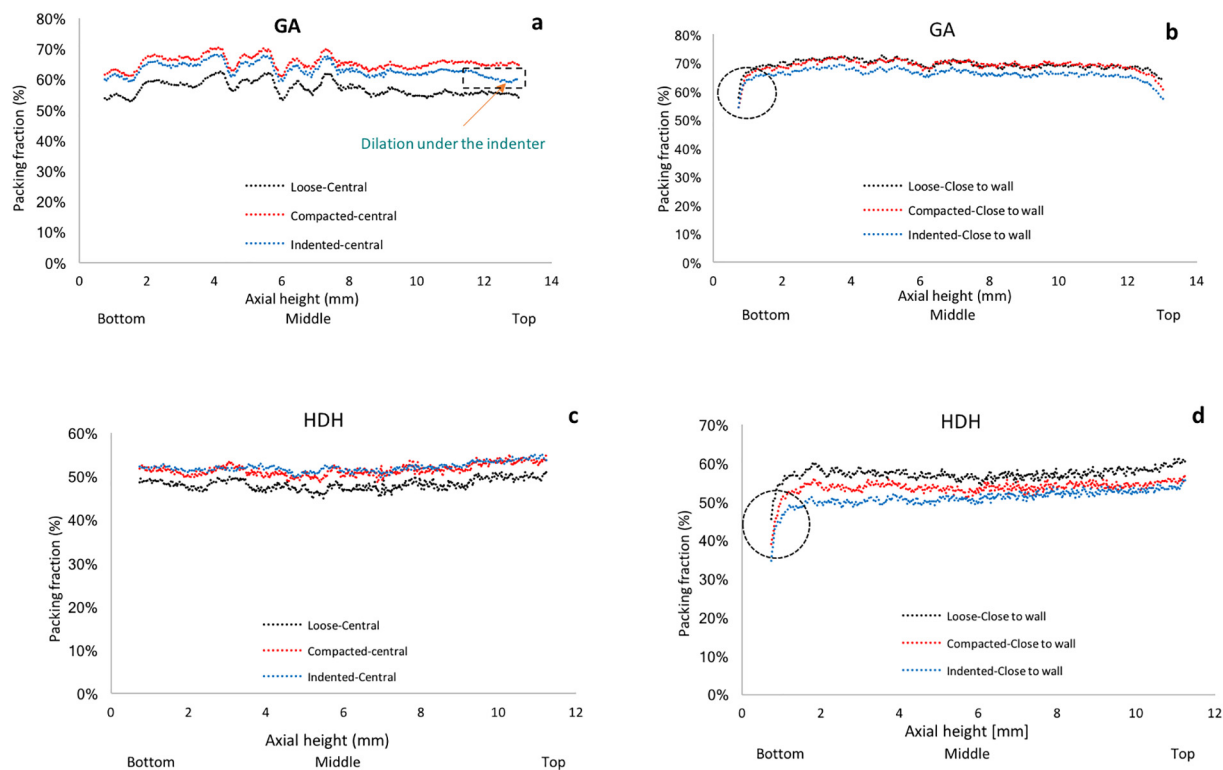


Fig. 22. Axial packing fraction for GA powder in (a) central zone and (b) wall zone and for HDH powder in (c) central zone and (d) wall zone at “loose-compacted-indented” stages.

- The analysis of equivalent diameter has shown that there is a slight difference between the volume equivalent and area equivalent sphere diameters for both powders due to the existence of internal pores and presence of concave/hollow particles for GA powders which could adversely affect the quality of final AM products.
- Quantitative analysis of powder packing fraction in radial (inner, outer and wall sections) and central zones at different axial (top, middle, and bottom sections) positions through the bed, for the filling, compaction and ball indentation stages has shown that the HDH powder has lower packing fraction than GA due to the difference in the shape and surface roughness.
- For both samples, there has been an increase of the packing fraction of the filling (loose) stage from the central zone towards the wall, due to a lower particle-wall CoF than that of particle-particle.
- In the central zone, after the compaction stage, the packing density has increased for both samples, however, for GA powder after removal of compaction pressure, there could have been a degree of bed expansion presumably due to the elastic recovery for the powder bed.
- During indentation, GA powder has also shown a slight reduction in the packing fraction just under the indenter due to the dilation of powder to accommodate shear. However, for the indentation stage the HDH powder has not shown a dilation under the indenter, suggesting the powder could be under a critically packed state, presumably due to their irregular shape.
- It has been observed that for loose or possibly very low compaction stages, the indentation position can have significant influence on the value of hardness for both powders, which is mainly due the differences in their particle shapes and coefficient of frictions.

CRediT authorship contribution statement

Mozhdeh Mehrabi: Conceptualization, Methodology, Investigation, Data curation, Visualization, Formal analysis, Writing - Original Draft.

Ali Hassanpour: Conceptualization, Methodology, Supervision, Writing - Reviewing and Editing.

Andrew Bayly: Supervision, Writing - Reviewing and Editing.

Declaration of Competing Interest

The authors declare that they have no known competing financial interests or personal relationships that could have appeared to influence the work reported in this paper.

Acknowledgments

The authors would like to acknowledge financial support from EPSRC-UK Future Manufacturing Hub in Manufacture using Advanced Powder Processes (MAPP) (EP/P006566/1, www.mapp.ac.uk).

References

- [1] I. Gibson, D.W. Rosen, B. Stucker, *Design for additive manufacturing*, Additive Manufacturing Technologies, Springer, Boston, MA 2010, pp. 299–332.
- [2] S. Haeri, Y. Wang, O. Ghita, J. Sun, Discrete element simulation and experimental study of powder spreading process in additive manufacturing, *Powder Technol.* 306 (2017) 45–54.
- [3] A.T. Sutton, C.S. Kriewall, M.C. Leu, J.W. Newkirk, Powder characterisation techniques and effects of powder characteristics on part properties in powder-bed fusion processes, *Virtual Physical Prototyp.* 12 (1) (2017) 3–29.
- [4] J. Tong, C.R. Bowen, J. Persson, A. Plummer, Mechanical properties of titanium-based Ti–6Al–4V alloys manufactured by powder bed additive manufacture, *Mater. Sci. Technol.* 33 (2) (2017) 138–148.
- [5] D. Geldart, E.C. Abdullah, A. Hassanpour, L.C. Nwoke, I.J.C.P. Wouters, Characterization of powder flowability using measurement of angle of repose, *China Particul.* 4 (03n04) (2006) 104–107.
- [6] H.H. Hausner, Powder characteristics and their effect on powder processing, *Powder Technol.* 30 (1) (1981) 3–8.
- [7] J.E. Peterson, W.M. Small, Evaluation of metal powders using Arnold density meter and Hall flowmeter, *Powder Metall.* 37 (1) (1994) 37–41.
- [8] R. Freeman, Measuring the flow properties of consolidated, conditioned and aerated powders—a comparative study using a powder rheometer and a rotational shear cell, *Powder Technol.* 174 (1–2) (2007) 25–33.

- [9] D. Schulze, Measuring powder flowability: a comparison of test methods-part I, *Powder Bulk Eng.* 10 (1996) 45–61.
- [10] M. Krantz, H. Zhang, J. Zhu, Characterization of powder flow: static and dynamic testing, *Powder Technol.* 194 (3) (2009) 239–245.
- [11] A.B. Spierings, M. Voegtlin, T. Bauer, K. Wegener, Powder flowability characterisation methodology for powder-bed-based metal additive manufacturing, *Progr. Addit. Manuf.* 1 (1–2) (2016) 9–20.
- [12] A. Hassanpour, M. Ghadiri, Characterisation of flowability of loosely compacted cohesive powders by indentation, *Part. Part. Syst. Charact.* 24 (2) (2007) 117–123.
- [13] C. Wang, A. Hassanpour, M. Ghadiri, Characterisation of flowability of cohesive powders by testing small quantities of weak compacts, *Particuology* 6 (4) (2008) 282–285.
- [14] U. Zafar, C. Hare, G. Calvert, M. Ghadiri, R. Girimonte, B. Formisani, M.A.S. Quintanilla, J.M. Valverde, Comparison of cohesive powder flowability measured by Schulze shear cell, raining bed method, Sevilla powder tester and new ball indentation method, *Powder Technol.* 286 (2015) 807–816.
- [15] Umair Zafar, Colin Hare, Ali Hassanpour, Mojtaba Ghadiri, Ball indentation on powder beds for assessing powder flowability: Analysis of operation window, *Powder Technol.* (2017) 300–306.
- [16] A. Du Plessis, I. Yadroitsev, I. Yadroitsava, S.G. Le Roux, X-ray microcomputed tomography in additive manufacturing: a review of the current technology and applications, *3D Print. Addit. Manuf.* 5 (3) (2018) 227–247.
- [17] K. Heim, F. Bernier, R. Pelletier, L.P. Lefebvre, High resolution pore size analysis in metallic powders by X-ray tomography, *Case Stud. Nondestruct. Test. Evaluat.* 6 (2016) 45–52.
- [18] F. Bernier, R. Tahara, M. Gendron, Additive manufacturing powder feedstock characterization using X-ray tomography, *Metal Powd. Rep.* 73 (3) (2018) 158–162.
- [19] R. Cunningham, A. Nicolas, J. Madsen, E. Fodran, E. Anagnostou, M.D. Sangid, A.D. Rollett, Analyzing the effects of powder and post-processing on porosity and properties of electron beam melted Ti-6Al-4V, *Mater. Res. Lett.* 5 (7) (2017) 516–525.
- [20] N. Bao, L. Shen, X. Feng, X. Lu, K. Yanagisawa, Shape and size characterization of potassium titanate fibers by image analysis, *J. Mater. Sci.* 39 (2) (2004) 469–476.
- [21] X. Fu, M. Dutt, A.C. Bentham, B.C. Hancock, R.E. Cameron, J.A. Elliott, Investigation of particle packing in model pharmaceutical powders using X-ray microtomography and discrete element method, *Powder Technol.* 167 (3) (2006) 134–140.
- [22] H. Hou, C.C. Sun, Quantifying effects of particulate properties on powder flow properties using a ring shear tester, *J. Pharm. Sci.* 97 (9) (2008) 4030–4039.
- [23] M. Bumiller, J. Carson, J. Prescott, A preliminary investigation concerning the effect of particle shape on a powder's flow properties, *World Congress on Particle Technology*, Vol. 4, 2002, July, pp. 21–25, Sydney Australia.
- [24] F. Podczeczek, Y. Mia, The influence of particle size and shape on the angle of internal friction and the flow factor of unlubricated and lubricated powders, *Int. J. Pharm.* 144 (2) (1996) 187–194.
- [25] W. Yu, K. Muteki, L. Zhang, G. Kim, Prediction of bulk powder flow performance using comprehensive particle size and particle shape distributions, *J. Pharm. Sci.* 100 (1) (2011) 284–293.
- [26] A.S. Chawanji, A.J. Baldwin, G. Brisson, E. Webster, Use of X-ray micro tomography to study the microstructure of loose-packed and compacted milk powders, *J. Microsc.* 248 (1) (2012) 49–57.
- [27] S.A. McDonald, P.J. Withers, Effect of punch shape on granular flow and rearrangement during powder compaction studied by X-ray microtomography, 7th World Congress on Industrial Process Tomography, WCIPT7, 2–5 September 2013, Poland, Krakow, 2013.
- [28] S.A. McDonald, L.C.R. Schneider, A.C.F. Cocks, P.J. Withers, Particle movement during the deep penetration of a granular material studied by X-ray microtomography, *Scr. Mater.* 54 (2) (2006) 191–196.
- [29] S.A. McDonald, F. Motazedian, A.C.F. Cocks, P.J. Withers, Shear cracking in an Al powder compact studied by X-ray microtomography, *Mater. Sci. Eng. A* 508 (1–2) (2009) 64–70.
- [30] A.G. Stavrou, C. Hare, A. Hassanpour, C.Y. Wu, Investigation of powder flowability at low stresses by DEM modelling, *Chem. Eng. Sci.* 211 (2020) 115307.
- [31] M. Pasha, C. Hare, A. Hassanpour, M. Ghadiri, Numerical analysis of strain rate sensitivity in ball indentation on cohesive powder beds, *Chem. Eng. Sci.* 123 (2015) 92–98.
- [32] B.S. Bass, Validating the Arcam EBM Process as an Alternative Fabrication Method for Titanium-6Al-4V Alloys, 2008.
- [33] G. Chen, P. Tan, S.Y. Zhao, W.W. He, H. Tang, Spherical Ti-6Al-4V powders produced by gas atomization, *Key Engineering Materials*, Vol. 704, Trans Tech Publications Ltd 2016, pp. 287–292.
- [34] J. Karlsson, A. Snis, H. Engqvist, J. Lausmaa, Characterization and comparison of materials produced by electron beam melting (EBM) of two different Ti-6Al-4V powder fractions, *J. Mater. Process. Technol.* 213 (12) (2013) 2109–2118.
- [35] A.C. Kak, M. Slaney, Principles of Computerized Tomographic Imaging, 2001 Society for Industrial and Applied Mathematics.
- [36] A. Sofou, G. Evangelopoulos, P. Maragos, Soil image segmentation and texture analysis: a computer vision approach, *IEEE Geosci. Remote Sens. Lett.* 2 (4) (2005) 394–398.
- [37] M. Veta, A. Huisman, M.A. Viergever, P.J. van Diest, J.P. Pluim, Marker-controlled watershed segmentation of nuclei in H&E stained breast cancer biopsy images, 2011 IEEE International Symposium on Biomedical Imaging: from Nano to Macro, IEEE 2011, March, pp. 618–621.
- [38] Y. Wang, C.L. Lin, J.D. Miller, 3D image segmentation for analysis of multisize particles in a packed particle bed, *Powder Technol.* 301 (2016) 160–168.
- [39] Y. Wang, C.L. Lin, J.D. Miller, Improved 3D image segmentation for X-ray tomographic analysis of packed particle beds, *Miner. Eng.* 83 (2015) 185–191.
- [40] C.L. Lin, J.D. Miller, Advances in X-ray computed tomography (CT) for improved coal washability analysis, International Coal Preparation Congress, 2010 Conference Proceedings, Society for Mining, Metallurgy & Exploration Inc, Englewood, CO 2010, pp. 888–897.
- [41] Y. Shi, W.M. Yan, Segmentation of irregular porous particles of various sizes from X-ray microfocus computer tomography images using a novel adaptive watershed approach, *Géotechn. Lett.* 5 (4) (2015) 299–305.
- [42] J. Fonseca, W.W. Sim, T. Shire, C. O'sullivan, Microstructural analysis of sands with varying degrees of internal stability, *Géotechnique* 64 (5) (2014) 405–411.
- [43] C.L. Lin, J.D. Miller, 3D characterization and analysis of particle shape using X-ray microtomography (XMT), *Powder Technol.* 154 (1) (2005) 61–69.
- [44] H.G. Merkus, Particle Size Measurements: Fundamentals, Practice, Quality, Vol. 17, Springer Science & Business Media, 2009.
- [45] Z. Liu, C. Huang, C. Gao, R. Liu, J. Chen, Z. Xiao, Characterization of Ti6Al4V powders produced by different methods for selective electron beam melting, *J. Min. Metall. B: Metallurgy* 55 (1) (2019) 121–128.
- [46] R. Cunningham, S.P. Narra, C. Montgomery, J. Beuth, A.D. Rollett, Synchrotron-based X-ray microtomography characterization of the effect of processing variables on porosity formation in laser powder-bed additive manufacturing of Ti-6Al-4V, *Jom* 69 (3) (2017) 479–484.
- [47] W.A. Gray, Packing of Solid Particles, 1968.
- [48] P. York, Particle slippage and rearrangement during compression of pharmaceutical powders, *J. Pharm. Pharmacol.* 30 (1) (1978) 6–10.
- [49] M. Alizadeh, A. Hassanpour, M. Pasha, M. Ghadiri, A. Bayly, The effect of particle shape on predicted segregation in binary powder mixtures, *Powder Technol.* 319 (2017) 313–322.
- [50] N.A. Armstrong, R.F. Haines-Nutt, Elastic recovery and surface area changes in compacted powder systems, *Powder Technol.* 9 (5–6) (1974) 287–290.
- [51] J. Berggren, G. Frenning, G. Alderborn, Compression behaviour and tablet-forming ability of spray-dried amorphous composite particles, *Eur. J. Pharm. Sci.* 22 (2–3) (2004) 191–200.
- [52] U. Zafar, Assessing flowability of cohesive powders by ball indentation (Doctoral dissertation, University of Leeds (School of Process, Environmental and Materials Engineering)), 2013.
- [53] A. Michrafy, J.A. Dodds, M.S. Kadiri, Wall friction in the compaction of pharmaceutical powders: measurement and effect on the density distribution, *Powder Technol.* 148 (1) (2004) 53–55.
- [54] Y. He, T.J. Evans, A.B. Yu, R.Y. Yang, DEM investigation of the role of friction in the mechanical response of powder compact, *Powder Technol.* 319 (2017) 183–190.